Regularly injected one-atom maser in the high-flux regime: a numerical study

G. M. D'Ariano, R. Seno, and N. Sterpi

Dipartimento di Fisica "A. Volta," Università degli Studi di Pavia, via Bassi 6, I-27100 Pavia, Italy

Received March 18, 1994; accepted August 31, 1994

We present a numerical study of the regularly injected one-atom maser in the high-flux regime, namely, when the time spacing between two consecutive injected atoms is comparable with the atom–field interaction time. Gain and losses are treated simultaneously in a general master equation that takes into account atomic incoherent decay. At stroboscopic times the dynamics of photon-number probability distribution is given by a suitably reduced Green operator, which has the form of a Markoff matrix. We perform a spectral analysis of the Green operator, showing the influence of photon traps on the eigenvalues. A comparison with the opposite case of Poissonian injection and low flux is given for a wide range of the pumping parameter θ. Regular injection leads to larger gain than Poissonian, but for high values of θ the opposite result can be found. Anomalous behaviors occur in which the normalized field fluctuations are increased by regularization of pumping and decreased by atomic decay: these features confirm similar anomalies found by other authors and are ascribed to the occurrence of nonclassical multiple-peak photon distributions and to different responses of the peaks to dissipation and gain. Atomic elastic collisions destroy any signature of trapping states on the stationary field. A comparison with a previously studied semiclassical model is given.

PACS numbers: 42.50.Dv, 42.50.Ar, 42.52.+x.

1. INTRODUCTION

The role of pumping statistics in the quantum dynamics of radiation in the one-atom maser[1–5] has been discussed by several authors.[6–11] In most of these papers[6–10] the limiting case of low atomic flux is considered; that is, the average time spacing τ_0 between two consecutively injected atoms is much larger than the flying time $\tau_{\rm int}$ in the cavity. This situation allows field decay to be neglected during the interaction with the atom. On the other hand, the case of high flux ($\tau_0 \approx \tau_{\rm int}$) is physically interesting also, because it approaches the situation that lies between those for the microscopic maser and the ordinary many-atom maser. There is, however, no theoretical treatment analogous to the case of low flux, because of the impossibility of separating the loss from the gain part of the density matrix evolution. In the research reported in Ref. 12 numerical results for the field dynamics were obtained in the framework of a semiclassical model. Reference 13 reports solutions for quasi-probability distributions in the Jaynes–Cummings model with photon damping, whereas in Ref. 14 an analytical solution of the micromaser master equation, based on direct diagonalization of the Liouvillian operator (with photon and atom damping) was presented.

In this paper we numerically evaluate the microscopic dynamics for the photon-number distribution of a quantized cavity mode in interaction with a beam of two-level atoms regularly injected into the cavity. We consider the high-flux regime, treating gain and dissipation simultaneously. The present approach is based on the evaluation of the joint radiation–atom Green operator that solves the microscopic master equation. The stroboscopic evolution of the field is then obtained from a suitably reduced Green operator, which has the form of a Markoff matrix. We give a spectral analysis of this matrix, emphasizing the influence of photon traps on the eigenvalues. First we study the dependence of the eigenvalues of the reduced Green operator on the parameters that characterize the system: the mean number of thermal photons $\bar{n}$, the number $N_{\rm ex} \equiv 1/2\gamma_c\tau_0$ of excited atoms crossing the cavity during the photon lifetime $(2\gamma_c)^{-1}$, and the pumping parameter $\theta \equiv g\tau_0\sqrt{N_{\rm ex}}$, where g is the atom–radiation coupling constant (the interaction time is assumed to be equal to the time spacing between two consecutive excited atoms in the beam, namely, $\tau_{\rm int} = \tau_0$). Then we focus attention on the stationary state of radiation, presenting numerical results in terms of mean photon numbers $\langle n\rangle$ and normalized fluctuations $\sigma = [\langle \Delta n^2\rangle/\langle n\rangle]^{1/2}$ for a wide range of the pumping parameter θ.

In the regime of negligible atomic decay the present regular-injection/high-flux case is compared with that of the standard one-atom maser, where the atomic beam is Poissonian and the flux is very low ($\tau_0 \gg \tau_{\rm int}$) (within this paper the two regimes are referred to as the RIHF and the PILF regimes, respectively). At very low temperatures we find some sizable differences between the fields obtained by the two schemes (for low-flux regularly injected masers, the same differences with respect to the standard one-atom maser were found[8]). For example, the fluctuations of radiation emitted in the RIHF regime are generally lower than those in the PILF case. However, for special ranges of θ, an anomalous increase in the normalized variance σ may be produced by regular pumping. For increasing temperature, quantitative differences are apparent for high values of θ, where, depending on the actual values of $N_{\rm ex}$ and θ, regular injection may lead to either higher or lower gain than does Poissonian injection. In both regimes, however, the threshold locations

0740-3224/95/020348-10$06.00

do not depend on injection: these and other similarities between the two injection schemes are ascribed to the fact that in both models the radiation interacts with no more than one atom at a time.

Regarding atomic decay, here we examine only processes involving two masing levels, neglecting decays toward other levels. Both coherence decay (decay of off-diagonal atomic matrix elements) at rate $\gamma_\perp$ and population decay at rate $\gamma_\parallel$ are considered. Physically these processes correspond to atomic collisions—either elastic or inelastic—with undesired atoms of different kinds that are present in the cavity without interacting with the radiation mode. In the radiative limit ($2\gamma_\perp = \gamma_\parallel$) atomic decay produces an enhancement of the photon distribution $p(n)$ at low n, and a corresponding reduction at high n, with an overall decrease of the mean photon number at steady state. For double-peaked photon distributions this mechanism may reduce σ, depending on the relative heights of the two peaks. This behavior is anomalous with respect to the customary probability broadening induced by atomic decay. The signature of trapping states on $p(n)$ is not affected by the atomic decay in the radiative limit, whereas it is washed out when elastic collisions are considered ($2\gamma_\perp > \gamma_\parallel$), because such collisions can produce hopping through the traps. In general, however, atomic decay produces sizable effects only for rates $\gamma_\parallel$ and $\gamma_\perp$ that are much greater than the cavity-damping constant.

After presenting the details of the microscopic approach, in Section 2 we perform a spectral analysis of the reduced Green operator. In Section 3 a comparison with the standard one-atom maser at steady state is given. In Section 4 the effects that are due to atomic decay are examined. A brief discussion of the present quantum model in comparison with a former semiclassical treatment[12] is presented in Section 5, where we show that agreement is found between conditionally stable classical fixed points and maxima of the quantum photon distribution. Section 6 concludes the paper, summarizing the results.

2. MASTER EQUATION

The evolution of the joint atom–radiation matrix $\hat{R}$ is described by the master equation in the interaction picture:

$$\frac{d\hat{R}}{dt} = \mathcal{L}\hat{R} \equiv -\frac{i}{\hbar}[\hat{H}_I, \hat{R}] + \mathcal{L}_f\hat{R} + \mathcal{L}_a\hat{R}, \tag{1}$$

where

$$\hat{H}_I = \hbar\delta a^\dagger a - i\hbar g(a\sigma_+ - a^\dagger\sigma_-), \tag{2}$$

$$\mathcal{L}_f\hat{R} = -\gamma_c(\bar{n}+1)(a^\dagger a\hat{R} + \hat{R}a^\dagger a - 2a\hat{R}a^\dagger) - \gamma_c\bar{n}(aa^\dagger\hat{R} + \hat{R}aa^\dagger - 2a^\dagger\hat{R}a), \tag{3}$$

$$\mathcal{L}_a\hat{R} = -\tfrac{1}{2}\gamma_\parallel[\sigma_+\sigma_-\hat{R} + \hat{R}\sigma_+\sigma_- - 2\sigma_-\hat{R}\sigma_+] - \tfrac{1}{4}(2\gamma_\perp - \gamma_\parallel)[\hat{R} - \sigma_z\hat{R}\sigma_z]. \tag{4}$$

The first term in Eq. (1) is the gain that is due to the atom–field interaction, here represented by the customary Jaynes–Cummings Hamiltonian [Eq. (2)] with coupling constant g and atom-field detuning δ; $\sigma_{x,y,z}$ are the Pauli spin matrices, $\sigma_\pm = (\sigma_x \pm i\sigma_y)/2$; a and $a^\dagger$ are the annihilation and creation operators, respectively, for the field mode. The second contribution, given in Eq. (3), describes the damping of the field in the cavity to a thermal distribution with average photon number $\bar{n}$. The term in Eq. (4) models atomic incoherent processes, i.e., population decay from the upper to the lower masing level with rate $\gamma_\parallel$ and polarization decay with rate $\gamma_\perp (2\gamma_\perp \geq \gamma_\parallel \geq 0)$. In presence of atomic collisions one has $\gamma_\parallel = \gamma_{\text{spont}} + \gamma_{\text{inel}}$ and $\gamma_\perp = \tfrac{1}{2}\gamma_\parallel + \gamma_{\text{el}}$ (γ_{inel} and γ_{el} are the contributions that are due to inelastic and elastic collisions, respectively; γ_{spont} is the spontaneous decay rate). In the one-atom maser spontaneous emission is suppressed; however, there is still the possibility of collisions with undesired atoms of different kinds in the cavity, and in addition Stark shifts that are due to electric fields at the borders of the cavity holes are also responsible for transverse decay. The case $2\gamma_\perp = \gamma_\parallel$ is usually referred to as the radiative limit, even though it occurs in the presence of inelastic collisions. Note that in our model the decay to atomic levels different from those of the masing couple is not taken into account: this mechanism would exclude the atom from the interacting dynamics, preventing it from reabsorbing radiation after decaying during the flying time.

At $t = 0$, namely, when the first atom enters the cavity, the joint density matrix is written in the factorized form

$$\hat{R}(0) = \hat{\rho}(0) \otimes |\uparrow\rangle\langle\uparrow|, \tag{5}$$

where $|\uparrow\rangle\langle\uparrow|$ denotes the upper masing state of the atom and $\hat{\rho}(0)$ is the initial state of the field. During the atom–field interaction the evolution of $\hat{R}(t)$ is governed by the Green operator $\exp(\mathcal{L}t)$ associated with Eq. (1):

$$\hat{R}(t) = \exp(\mathcal{L}t)\hat{R}(0) \qquad (0 \leq t < \tau_0). \tag{6}$$

When the atom leaves the cavity, at $t = \tau_0$, one obtains the state of the field by tracing $\hat{R}(t)$ over the atomic Hilbert space. At the same time (more precisely, at the time $t = \tau_0 + 0^+$ immediately after) a new atom enters the cavity in the excited state, and correspondingly a new initial condition is imposed:

$$\hat{R}(\tau_0) = \mathrm{Tr}_a\{\exp(\mathcal{L}\tau_0)\hat{R}(0)\} \otimes |\uparrow\rangle\langle\uparrow| \equiv \hat{\rho}(\tau_0) \otimes |\uparrow\rangle\langle\uparrow|. \tag{7}$$

If all forthcoming atoms are entering the cavity at stroboscopic times $t_n = n\tau_0$, one has

$$\hat{R}(n\tau_0) = \mathrm{Tr}_a\{\exp(\mathcal{L}\tau_0)\hat{R}[(n-1)\tau_0]\} \otimes |\uparrow\rangle\langle\uparrow|, \tag{8}$$

and, at a generic time t $(n\tau_0 < t < (n+1)\tau_0)$,

$$\hat{R}(t) = \exp[\mathcal{L}(t - n\tau_0)]\hat{R}(n\tau_0). \tag{9}$$

One obtains the reduced density matrix that describes the field $\hat{\rho}(t)$ on partially tracing $\hat{R}(t)$ over the atomic variables:

$$\hat{\rho}(t) = \mathrm{Tr}_a[\hat{R}(t)]. \tag{10}$$

It is convenient to decompose the density matrix $\hat{R}(t)$ as follows:

$$\hat{R}(t) = \sum_{k=-\infty}^{+\infty} \sum_{n=\max(0,k)}^{+\infty} X_n^{(k)}(t)|n\rangle\langle n-k| \otimes |\downarrow\rangle\langle\downarrow| + Y_n^{(k)}(t)|n\rangle\langle n-k| \otimes |\uparrow\rangle\langle\uparrow| + \tfrac{1}{2} Z_n^{(k)}(t)\{|n\rangle\langle n-k+1| \otimes |\uparrow\rangle\langle\downarrow| + \text{H.c.}\}. \quad (11)$$

The index k in Eq. (11) is left invariant under the action of the Liouvillian operator in Eq. (1). The matrix representation $\mathbf{L}_k$ of the Liouvillian $\mathcal{L}$ for fixed k is defined according to the equation

$$\frac{\mathrm{d}}{\mathrm{d}t}[\ldots, X_n^{(k)}, Y_n^{(k)}, Z_n^{(k)}, X_{n+1}^{(k)}, Y_{n+1}^{(k)}, Z_{n+1}^{(k)}, \ldots]^T = \mathbf{L}_k[\ldots, X_n^{(k)}, Y_n^{(k)}, Z_n^{(k)}, X_{n+1}^{(k)}, Y_{n+1}^{(k)}, Z_{n+1}^{(k)}, \ldots]^T, \quad (12)$$

where T indicates a vertical (transposed) vector. If the initial state $\hat{\rho}(0)$ of the field is diagonal in the number representation, the dynamics takes place only in the sector with $k = 0$, and the matrix $\mathbf{L}_0$ is given by Eq. (13) (page 351), where we have introduced the scaled quantities

$$W \equiv \gamma_{\parallel}/2\gamma_c, \qquad \gamma \equiv \gamma_{\perp}/2\gamma_c. \quad (14)$$

A. Reduced Green Operator

In what follows, we examine only the strobscopic evolution of the field density matrix: Eq. (8) can be written in terms of a reduced Green operator $\exp(\mathcal{R}\tau_0)$, which directly gives the field density matrix as follows:

$$\exp(\mathcal{R}\tau_0)\hat{\rho}[(n-1)\tau_0] = \hat{\rho}[n\tau_0]. \quad (15)$$

From Eqs. (8) and (10) it follows that the reduced Green operator can be written in form of a partial trace over the atomic Hilbert space:

$$\exp(\mathcal{R}\tau_0) = \mathrm{Tr}_a\{\exp(\mathcal{L}\tau_0)(\hat{1} \otimes |\uparrow\rangle\langle\uparrow|)\}. \quad (16)$$

The Green operator $\exp(\mathcal{L}\tau_0)$ is evaluated in the sector with $k = 0$ when the matrix $\mathbf{L}_0$ is diagonalized numerically, and then the reduced operator $\exp(\mathcal{R}\tau_0)$ is obtained after the partial trace [Eq. (16)]. It should be emphasized that the present approach is numerically efficient, especially if compared with more time-consuming algorithms, for example, direct integration of the master equation. In fact, one should note that the Green operator contains all the information about the stroboscopic field evolution and the stationary state itself, and any property of the field can be evaluated quickly after the matrix representation of $\exp(\mathcal{R}\tau_0)$ is saved. There are, however, precision limits that arise from the fact that the matrix $\mathbf{L}_0$ is not Hermitian, and some eigenvectors become too close to one another for increasing dimensions of truncated Hilbert space (analogous precision problems arise in the analytical approach of Ref. 14). In practice, we obtain acceptable results for no more than 60 photons in the cavity, using standard double-precision algorithms.

The stationary states are, by definition, the eigenvectors corresponding to unit eigenvalues of $\exp(\mathcal{R}\tau_0)$. At this point some remarks are in order regarding the degeneracy of the unit eigenvalue and, more generally, the spectrum of the reduced Green operator. The operator $\exp(\mathcal{R}\tau_0)$ propagates the photon probability distribution $\langle m|\hat{\rho}[n\tau_0]|m\rangle$, and hence it is a Markoff matrix; that is, the sum of elements on each column is unity. For any generic Markoff matrix the moduli of all eigenvalues λ_i are $|\lambda_i| \leq 1$. The unit eigenvalue can be degenerate: moreover, some eigenvalues can be equal to complex roots of unity. For a degenerate unit eigenvalue the stationary state is not unique; that is, the long-time solution depends on the initial condition. On the other hand, if there are complex roots of unity, then the corresponding eigenvectors represent cyclic or quasi-periodic states, depending on whether the root is rational or irrational. In the finite-dimensional case there is a simple theorem[15] that guarantees the existence and uniqueness of the stationary state for strictly positive Markoff matrices. In our case, however, the matrix is infinite, and the necessary dimensional truncation affects the normalization, so that $\exp(\mathcal{R}\tau_0)$ is actually a quasi-Markoff matrix. For $\gamma_c > 0$ an extensive numerical analysis shows that eigenvalues that are complex roots of unity never occur. The complex eigenvalues of a large set of Markoff matrices are plotted in Fig. 1 for $\theta \in [0, 20]$, $N_{\mathrm{ex}} = 20$, $\bar{n} = 0$, and $W = \gamma = 0$ (we verified that the unit eigenvalue is always nondegenerate). From the above observations one concludes that there are no stroboscopically oscillating photon states—neither cyclic nor quasi-periodic—and that the stationary state is independent of the initial condition. It is clear that this quantum situation is quite different from the semiclassical one, in which all kinds of oscillating states are possible and the stationary field depends on the initial condition (see Ref. 12 for regular injection and Refs. 16 and 17 for Poissonian injection).

B. Trapping States

For $\gamma_c = \gamma_{\parallel} = \gamma_{\perp} = 0$, unlike for the lossy case, the unit eigenvalue of the Markoff matrix may be degenerate, in correspondence to the so-called trapping states.[18,19] The trapping states are number eigenstates $|l\rangle$ such that the atom undergoes an integer number of Rabi flops, namely,

$$q\pi = \theta[(l+1)/N_{\mathrm{ex}}]^{1/2}. \quad (17)$$

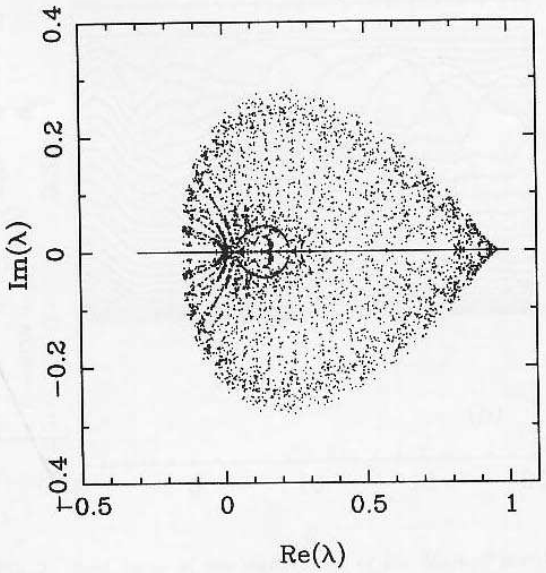

Fig. 1. Eigenvalues of a sample of Markoff matrices with $\theta \in [0, 20]$, $N_{\mathrm{ex}} = 20$, $\bar{n} = 0$, and $W = \gamma = 0$ (the resolution in θ is 0.01). No eigenvalue falls out of the plotted window.

$$
\mathbf{L}_0 = 2\gamma_c
\begin{bmatrix}
\cdots & \cdots & \cdots & \cdots & \cdots & \cdots & \cdots \\
\cdots & -\overline{n}(2n+1) - n & W & 0 & -\frac{g}{\gamma_c}\sqrt{n+1} & (\overline{n}+1)(n+1) & \cdots \\
\cdots & 0 & -\overline{n}(2n+1) - n - W & \frac{g}{2\gamma_c}\sqrt{n+1} & -2\overline{n}(n+1) - (n+1/2) - \gamma & -\frac{g}{2\gamma_c}\sqrt{n+1} & 0 \\
\cdots & 0 & \frac{g}{2\gamma_c}\sqrt{n+1} & \overline{n}(n+1) & \frac{g}{\gamma_c}\sqrt{n+1} & 0 & (\overline{n}+1)(n+1) \\
\cdots & \overline{n}(n+1) & 0 & 0 & \frac{g}{\gamma_c} & 0 & 0 \\
\cdots & 0 & \overline{n}(n+1) & 0 & 0 & 0 & 0 \\
\cdots & 0 & 0 & 0 & \overline{n}\sqrt{(n+1)(n+2)} & 0 & 0 \\
\cdots & \cdots & \cdots & \cdots & \cdots & \cdots & \cdots
\end{bmatrix}
\tag{13}
$$

If there is a couple of integers (q, l) that satisfy Eq. (17) for some θ and N_{ex}, then there exists an infinite set of integer couples $\{(q, l)\}$ that satisfy Eq. (17) for the same fixed θ and N_{ex}: all states $\{|l\rangle\}$ are trapping states corresponding to degenerate eigenvectors for $\lambda = 1$. In this situation the stationary field is a mixture of trapping states, with probabilities depending on the initial condition.

For nonvanishing γ_c the degeneracy is removed. However, there is reminiscence of the trapping states, because for the same special values[20] of θ in Eq. (17) some eigenvalues now become *nearly* degenerate with $\lambda = 1$. This is evident from Fig. 2(a), where the same eigenvalues of Fig. 1 are now plotted versus θ. The quasi-degeneracy is interpreted as follows: For $\gamma_c > 0$ the trapping integers l remain barriers in Hilbert space (hereafter referred to as traps): because of damping the traps can be crossed in the direction of lower photon numbers. Photon probability flow across the barriers in the increasing photon-number direction can occur as a consequence of thermal hopping for $\bar{n} > 0$. As a consequence of the crossing mechanisms the trapping eigenvectors now become nonprobabilistic states (nonpositive-definite eigenvectors), whose eigenvalues remain close (but not equal) to 1. Increasing the temperature [see Fig. 2(b)] removes this quasi-degeneracy. From the above considerations one concludes that the traps will also influence the stationary state for nonvanishing damping, the effect being more sizable near the trapping condition and for low thermal photons $\bar{n}$.

3. REGULAR VERSUS POISSON INJECTION

In this section we analyze the cavity photon statistics at stroboscopic steady state for vanishing atomic decay. The results are compared with those from the standard one-atom maser[2–4] for the same values of θ and N_{ex}. The shapes of the photon probability distributions $p(n)$ are influenced by the presence of traps, which depend not on injection but just on the condition that there is only one atom in the cavity at a time. In spite of this common feature, sizable differences between the normalized variances of the two schemes are found.

A. Zero Temperature

In Fig. 3(a) we show the normalized average number of photons $\langle n\rangle/N_{ex}$ in the RIHF regime as a function of the pumping parameter θ for $\bar{n} = 0$ and $N_{ex} = 20$. The photon distribution $p(n)$ is superimposed in gray scale. It is apparent that the cavity field presents features very similar to those obtained in the regularly injected low-flux regime previously studied by Guerra *et al.*[8] This happens even though, for low atomic flux, gain and loss are factorized during the atom–field interaction. One can see that the mean photon number exhibits a highly singular behavior, presenting sharp drops where the photon probability distribution is abruptly truncated. The reason for the $p(n)$ truncation is easily explained in terms of traps, i.e., barriers in the Fock space that correspond to trapping states that for zero thermal photons can be crossed only toward lower photon numbers and hence abruptly truncate the photon probability distribution. Figure 3(b) shows the photon probability distribution that corresponds to the case in Fig. 3(a) but in the PILF regime. One can note strong similarities in the mean photon number, even though the physical situations and the theoretical treatments are widely different. The location of traps is shifted by the value $\Delta\theta/\theta = 1/[32N_{ex}\theta^2(n_\theta + 1)]$ as a result of damping shift of the Rabi frequency[20]; however, for our choice of parameters, $\Delta\theta/\theta$ is very small and is not visible in the plots (for example, $\Delta\theta/\theta \simeq 10^{-6}$ for $N_{ex} = 20$, $\theta = 8$ at a two-photon trap; the shift would become more relevant for decreasing N_{ex} and θ).

With regard to the photon normalized variance versus θ, quick alternation between sub-Poissonian and super-Poissonian photon statistics is found, as in the

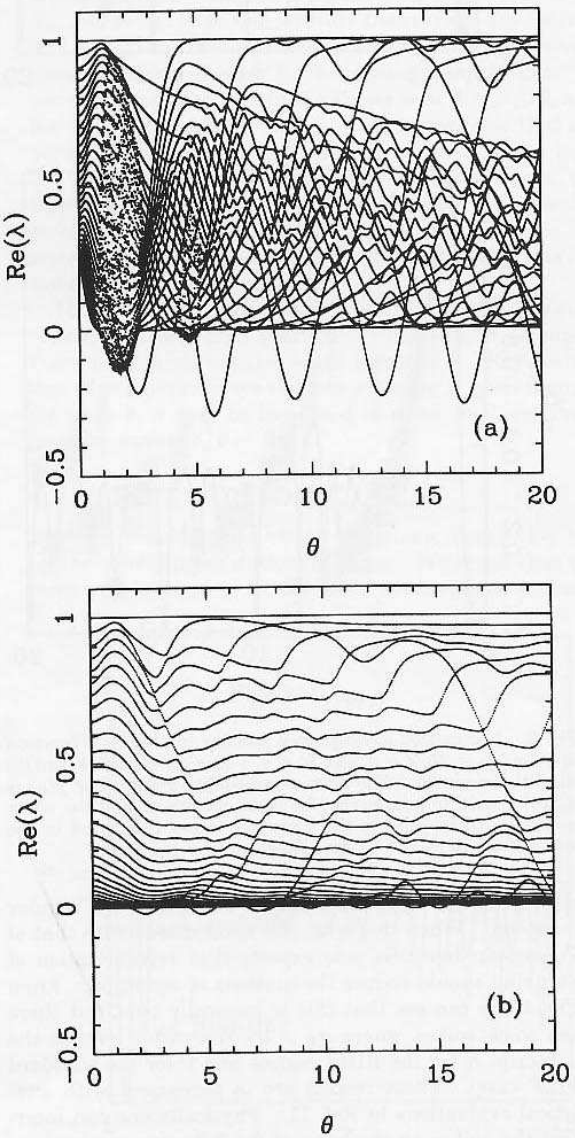

Fig. 2. Real parts of the eigenvalues of the Markoff matrix versus the pumping parameter θ for (a) the same parameters as in Fig. 1 and (b) for the same parameters as in (a) but with $\bar{n} = 1$.

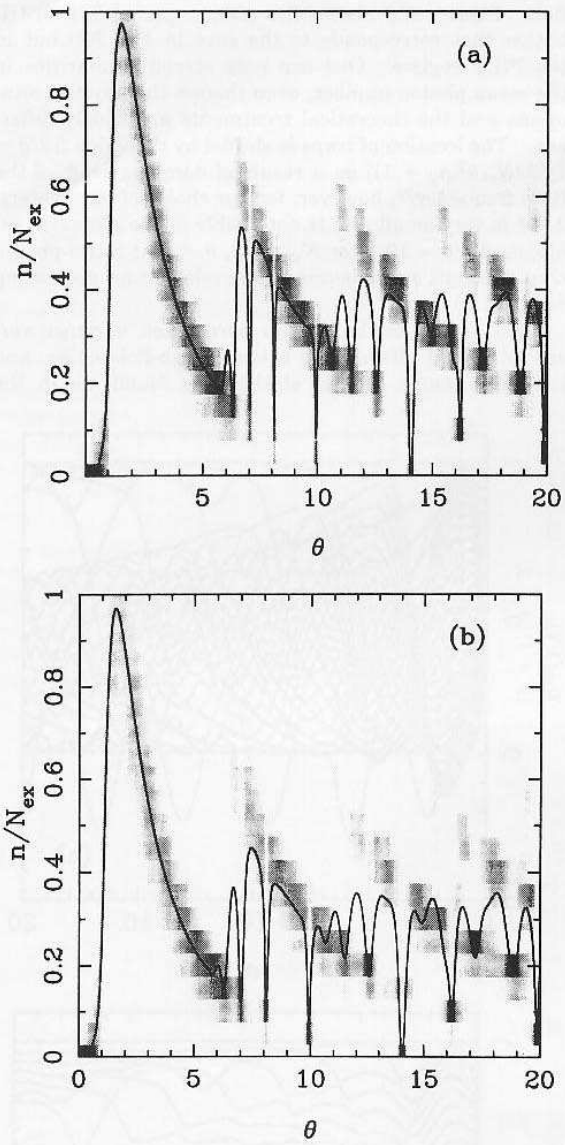

Fig. 3. Normalized mean photon number $\langle n\rangle/N_{ex}$ as a function of θ for $N_{ex} = 20$, $\bar{n} = 0$, and $W = \gamma = 0$, in (a) the RIHF and (b) the PILF regimes. The photon probability distribution $p(n)$ is superimposed in gray scale (the black maximum and the white minimum correspond to the extremal values calculated in the whole interval of θ's). (The resolution in θ is 0.01.)

regime of low flux and either Poissonian or regular pumping. When this situation is compared with that of Poissonian injection, one expects that regularization of pumping should reduce fluctuations of radiation. From Fig. 4 one can see that this is generally true, but there are some spikes where $\sigma_R > \sigma_P$ (hereafter we use the subscript R for the RIHF regime and P for the standard PILF case). These results are in agreement with analytical evaluations in Ref. 11. Physically one can interpret the spikes on the basis of the following mechanism. Let us consider, for example, the case with $\theta = 7.99$ in Figs. 5(a) and 5(b). For Poisson injection [Fig. 5(b)] the photon probability distribution $p(n)$ presents two peaks of comparable height. In the RIHF regime the gain mechanism is more efficient; thus $p(n)$ is still double peaked, but the peak for nine photons is much higher than that for two photons, leading to higher $\langle n\rangle$ and lower Δn^2 so that $\sigma_R < \sigma_P$. An opposite result is obtained when the first peak is much higher than the second one. This is the case for $\theta = 8.09$ in Figs. 5(c) and 5(d). As a result of regular injection, the peak for nine photons is higher than in the Poissonian case, so that the photon uncertainty is larger. The mean photon number is larger too, but now $\sigma_R > \sigma_P$, because number fluctuations are more sensitive to the second peak. Hence the anomalous behavior

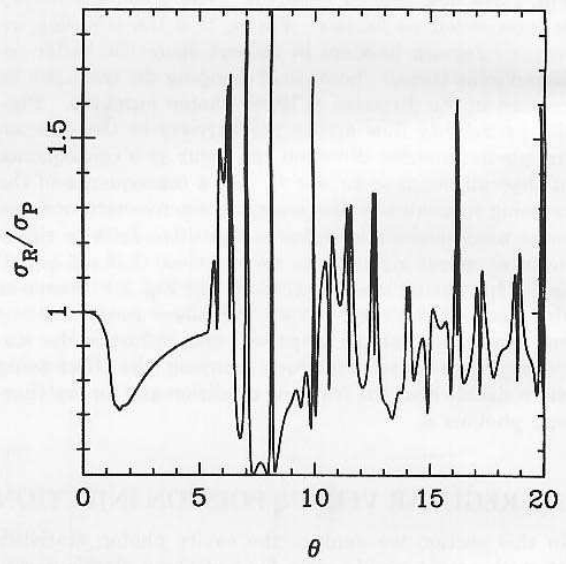

Fig. 4. Ratio of the normalized variances σ_R/σ_P for the same parameters as in Fig. 3.

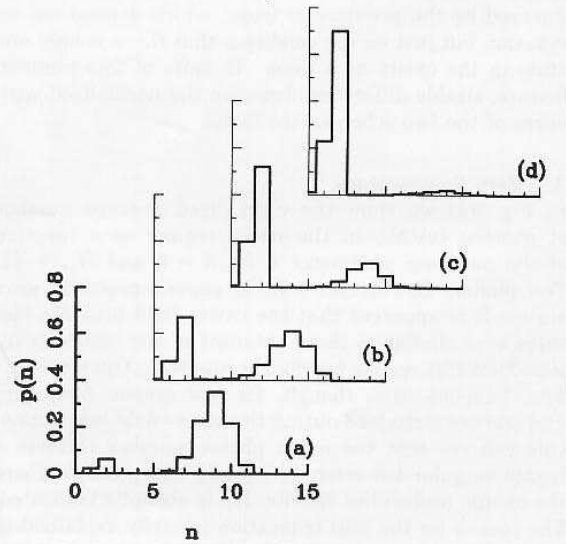

Fig. 5. Histograms of the stationary photon distributions for $\theta = 7.99$ in (a) the RIHF and (b) the PILF regimes and for $\theta = 8.09$ in (c) the RIHF and (d) the PILF regimes. The other parameters are $N_{ex} = 20$, $\bar{n} = 0$, and $W = \gamma = 0$.

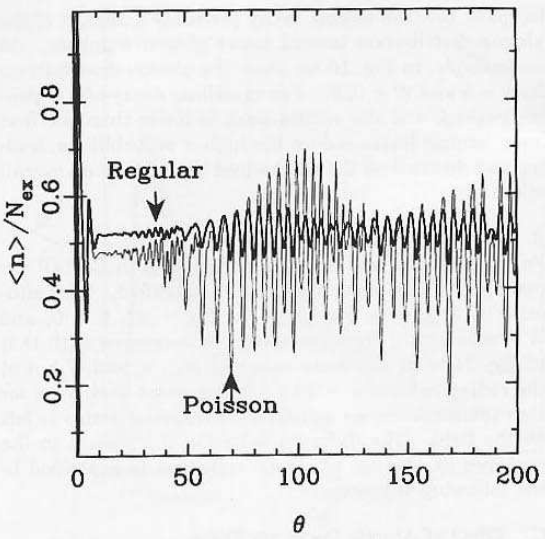

Fig. 6. Normalized mean photon number $\langle n\rangle/N_{ex}$ versus θ in the RIHF and the PILF regimes for $N_{ex} = 20$, $\bar{n} = 1$, and $W = \gamma = 0$.

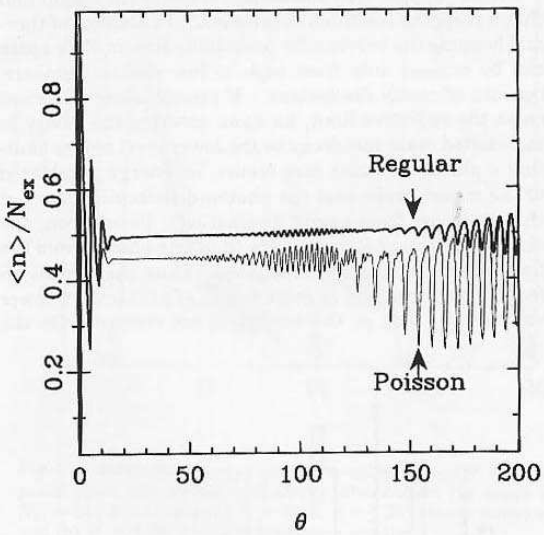

Fig. 7. Normalized mean photon number $\langle n\rangle/N_{ex}$ versus θ in the RIHF and the PILF regimes for $N_{ex} = 50$, $\bar{n} = 1$, and $W = \gamma = 0$.

of σ_R/σ_P is due to a different response of the peaks of $p(n)$ to dissipation and gain: this happens both in the high-flux and in the low-flux[8] regimes.

B. Nonzero Temperature

The main features of the stationary field change drastically with increasing temperature. In fact, all singular behaviors of $\langle n\rangle$ and σ are washed out by thermal hopping. There are quantitative differences between the RIHF and the PILF regimes: regular pumping with high flux may lead to either larger or lower radiation intensities. In particular, it originates higher gain in a range of θ that increases with N_{ex} (see Figs. 6 and 7). However, for $\theta \gg N_{ex}$ the mean photon number versus θ presents high amplitude oscillations that are much less pronounced in the RIHF than in the PILF regime, especially for $N_{ex} = 20$. This produces a lower mean photon number in the RIHF regime. We have no intuitive understanding of the less efficient gain mechanism, which is apparent in Fig. 6.

As regards the oscillations of $\langle n\rangle$ versus θ, we notice a multiple structure of collapses with revivals. This is a different behavior with respect to the PILF regime, where only one collapse with a nondecaying revival[3] is observed. The multiple structure of collapses with revivals is more apparent with increasing N_{ex} (see Fig. 7), and in this case the oscillations are more regular. The values of θ at which multiple collapses with revivals occur depend on N_{ex} and $\bar{n}$: at fixed temperature the revivals are delayed in θ if N_{ex} is increased, whereas for fixed N_{ex} the revivals merge into one another for decreasing temperature. In the case presented, the first collapse is at $\theta \simeq N_{ex}/2$, and the revival occurs at $\theta \simeq N_{ex}$. It is remarkable that the period of oscillation of $\langle n\rangle$ versus θ is the same for both the RIHF and the PILF regimes. In other words, the threshold locations do not depend either on the injection or on the flux. In particular, for $\theta \leq 5$ (i.e., up to the second threshold) the average field intensity also has the same value.

The normalized variance is shown in Fig. 8. Because of the relatively high thermal fluctuations, σ is super-Poissonian in almost the whole range of θ. Regularization of pumping always reduces σ for low θ, even though, for large θ, σ may be increased in some small intervals (see, for example, $\theta \simeq 65$).

4. EFFECT OF ATOMIC DECAY

We now consider the effects of atomic decay [Eq. (4)] on the stroboscopic stationary state. We recall that the term proportional to $\gamma_\parallel$ describes spontaneous emission

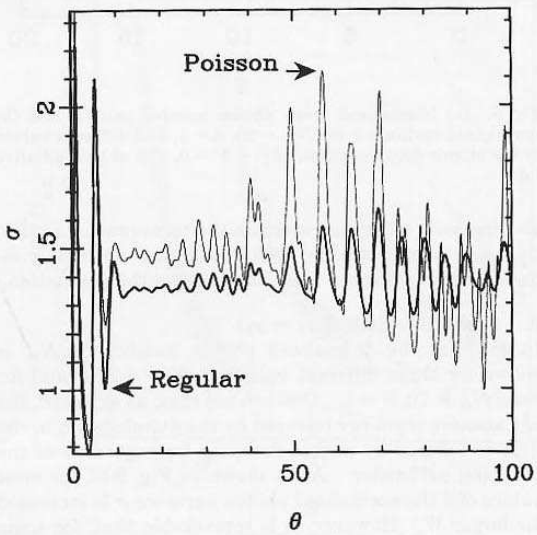

Fig. 8. Normalized variances in the RIHF and the PILF regimes for the same parameters as for Fig. 6.

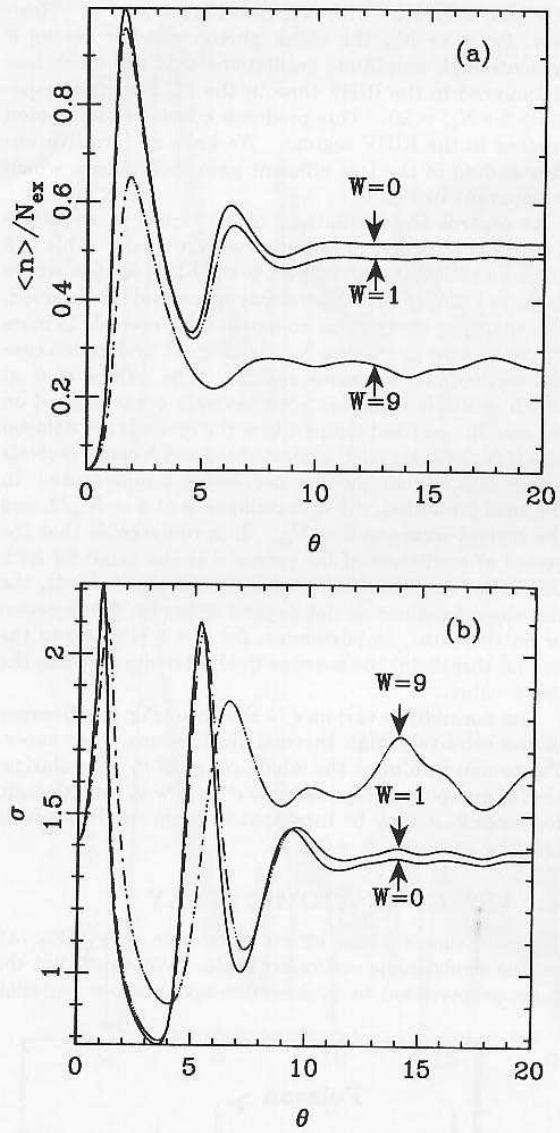

Fig. 9. (a) Normalized mean photon number $\langle n\rangle/N_{ex}$ and (b) normalized variance σ for $N_{ex} = 20$, $\bar{n} = 1$, and different values of the atomic decay constants $2\gamma = W = 0, 1, 9$ at the radiative limit.

and inelastic collisions, whereas the term proportional to $2\gamma_\perp - \gamma_\parallel$ is originated by elastic collisions, which only reduce atomic coherence without changing the population.

A. Radiative Limit ($2\gamma_\perp = \gamma_\parallel$)

In Fig. 9(a) the normalized photon number $\langle n\rangle/N_{ex}$ is shown for three different values of $W = \gamma_\parallel/2\gamma_c$ and for fixed $N_{ex} = 20$, $\bar{n} = 1$. One can see that, as expected, the net amount of energy released by the atomic beam to the field is reduced by atomic damping for any value of the pumping parameter. As is shown in Fig. 9(b), for most values of θ the normalized photon variance σ is increased for larger W. However, it is remarkable that, for some values of the pumping parameter, the opposite situation may occur, namely, σ is reduced for increasing W. This happens because atomic decay produces a spread of the photon distribution toward lower photon numbers. As an example, in Fig. 10 we show the photon distributions for $\theta = 5$ and $W = 0, 9$. For vanishing decay $p(n)$ is double peaked, and the second peak is lower than the first one: atomic losses reduce the high-n probabilities, leading to a decrease of the normalized variance as an overall effect.

B. Elastic Collisions ($2\gamma_\perp > \gamma_\parallel$)

For elastic collisions [see the second term in Eq. (4)] the main features of $p(n)$ are drastically modified. This situation is shown in Fig. 11(a) for $N_{ex} = 20$, $\bar{n} = 0$, and $W = \gamma = 6.28$. This plot should be compared with that in Fig. 11(b) for the same values of N_{ex}, $\bar{n}$, and W but at the radiative limit $\gamma = 3.14$. It is evident that, even for zero temperature, no signature of trapping states is left on the field. The different behavior of the field in the presence or absence of elastic collisions is explained in the following subsection.

C. Effect of Atomic Decay on Traps

In this subsection we briefly illustrate the different kinds of atomic decay mechanism and their effect on photon traps.

Let us suppose that the atomic decay is turned off and that a trapping condition is satisfied. In absence of thermal hopping the barriers for probability flow in Fock space can be crossed only from high to low photon numbers, because of cavity dissipation. If atomic decay is turned on in the radiative limit, an atom entering the cavity in the excited state can decay to the lower level before emitting a photon. If this case occurs, no energy is released to the maser mode, and the photon distribution does not change, apart from cavity dissipation. In addition, the same atom can absorb no more than one photon from the field before leaving the resonator. Thus the overall effect of this process is at most a shift of $p(n)$ toward lower values of n; that is, the barrier is not crossed. On the

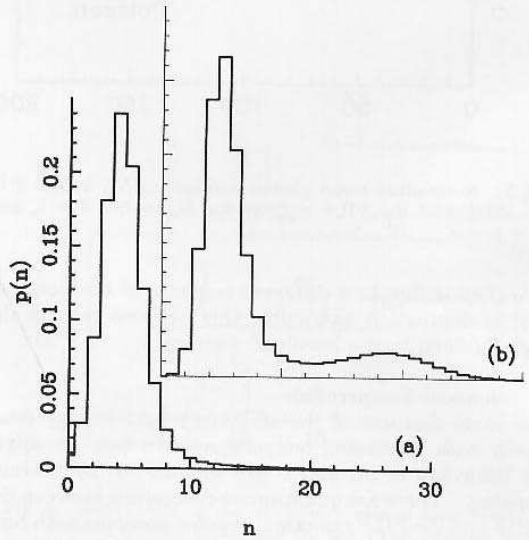

Fig. 10. Photon probability distributions for $\theta = 5$, $N_{ex} = 20$, $\bar{n} = 1$, and (a) $W = 9$ and (b) $W = 0$ at the radiative limit.

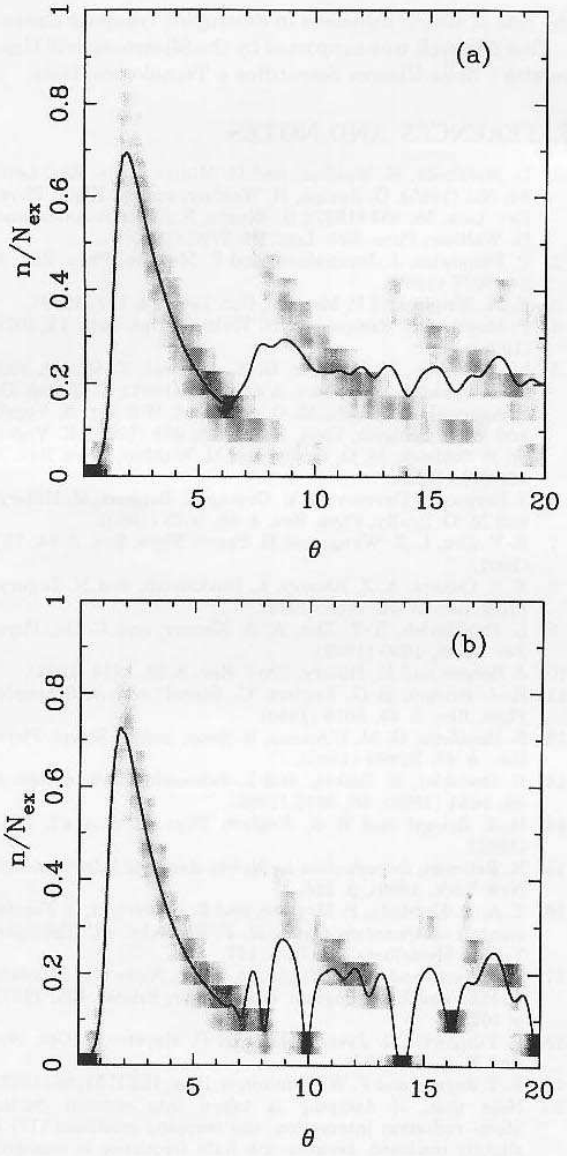

Fig. 11. Normalized mean photon number versus θ superimposed upon the photon probability distribution (in gray) for $N_{ex} = 20$, $\bar{n} = 0$, and (a) $W = 6.28$, $\gamma = 6.28$ (elastic collisions) and (b) $W = 6.28$, $\gamma = 3.14$ (radiative limit).

other hand, for elastic collisions it may happen that an atom entering the cavity emits a photon and later is subject to a collision, changing the atomic coherence. If this occurs, it may happen that the atom is prevented from reabsorbing a photon before leaving the cavity. In this process the barrier for the photon probability is crossed toward higher photon numbers, and this basically explains why no trace of trapping states is left on the field. These results are in agreement with those in Ref. 11.

5. QUANTUM VERSUS SEMICLASSICAL DYNAMICS

A strict comparison between semiclassical quantities and the corresponding quantum averages is meaningful only for single-peaked probability distributions and for short interaction times. At steady state a comparison is still possible only if a small number of Rabi turns is considered. In fact, for long times or large Rabi angles the quantum atom–field correlation becomes relevant in determining the final features of the field. Moreover, we emphasize that the quantum model always leads to a unique steady state, whereas semiclassically there are many different long-time solutions, depending on the initial condition. With the above considerations in mind, in this section we compare the steady state of the present model with that of a previous semiclassical analysis[12] in the RIHF regime. We consider zero temperature and vanishing atomic damping.

In Ref. 12 the dynamics of the field amplitude $a(t)$ is described by an integrodifferential equation that resembles a kicked, damped pendulum equation. At stroboscopic steady state, when the time fluctuations of $a(t)$ are neglected, the temporal average $\bar{a}$ in a fly-time interval τ_0 satisfies the following relation[21]:

$$\sin^2(g\tau_0\bar{a}) - \frac{1}{N_{ex}}\bar{a}^2 = 0. \tag{19}$$

The roots of Eq. (18) can be either unstable or conditionally stable.[16,17] The conditionally stable roots are fixed points of the evolution; that is, they represent the classical stroboscopic steady states. These points are conditionally stable because they are replaced by chaotic attractors by an increase in the pumping parameter. When this replacement occurs, the field in the cavity is stroboscopically oscillating, and one can have either cyclic or quasiperiodic states, the actual long-time solution depending on the initial condition.

In Fig. 12 we show the stationary photon probability distribution $p(n)$ for $N_{ex} = 20$ along with the conditionally stable fixed points of Eq. (18). One can see that the fixed-point solutions of the semiclassical model are

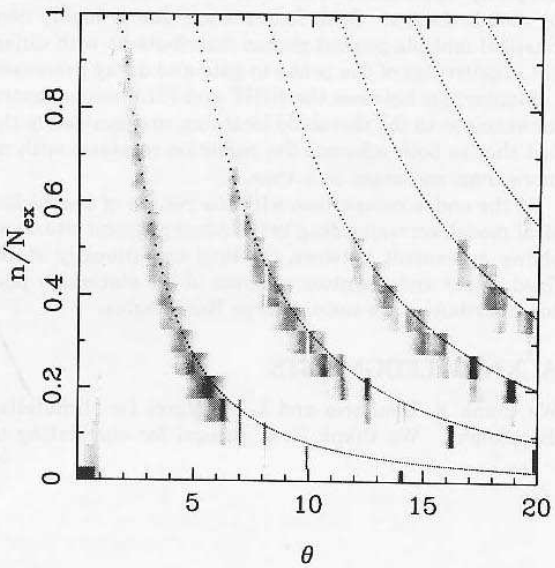

Fig. 12. Conditionally stable fixed points of the semiclassical evolution (dots) superimposed upon the stationary photon probability distribution (in gray) for $N_{ex} = 20$, $\bar{n} = 0$, and $W = \gamma = 0$.

close to the maxima of the photon distribution, even for multiple-peaked probabilities. Thus, when $p(n)$ has only one peak, the quantum mean photon number can be reproduced well by the semiclassical intensity for a proper choice of the initial condition. However, when $p(n)$ has two peaks of comparable height the value of the mean photon number lies between the peaks, and the semiclassical intensity cannot fit the stationary quantum average [compare Fig. 3(a) with Fig. 12]. Similar results were obtained in the research reported in Ref. 22 in the framework of a Fokker–Planck approach to the PILF one-atom maser.

6. CONCLUSIONS

In this paper we have presented numerical results for the stationary photon distribution in a regularly injected micromaser for high flux, namely, when the time spacing between two consecutive excited atoms is constant and comparable with the atom–field interaction time. In our approach both gain and losses are treated simultaneously in a dynamical evolution governed by a general microscopic master equation, which also takes into account incoherent decay processes for the atom. We evaluated the stroboscopic steady state by diagonalizing the reduced Green operator, and we analyzed the dependence of the eigenvalues on the pumping parameter.

In comparison with the standard one-atom maser, we find that the micromaser in the RIHF regime generally originates a more efficient gain mechanism, but it also may lead to lower gain, depending on the actual values of N_{ex} and θ. For the dependence of the mean photon number on the pumping parameter, a multiple structure of collapses with revivals is found. Traps are destroyed by atomic elastic collisions.

The normalized intensity fluctuations are generally lower in the RIHF than in the PILF regime. However, anomalous behaviors can be found for special ranges of the pumping parameter, where fluctuations are decreased by atomic decays. Such features are due to highly nonclassical mutiple-peaked photon distributions with different sensitivities of the peaks to gain and decay processes.

Similarities between the RIHF and PILF micromasers, for example, in the threshold locations, are ascribed to the fact that in both schemes the radiation interacts with no more than one atom at a time.

In the end, a comparison with the results of a semiclassical model, corresponding to the same physical situation, shows agreement between classical conditionally stable fixed points and quantum maxima of the stationary photon distribution for not-too-large Rabi angles.

ACKNOWLEDGMENTS

We thank R. Bonifacio and L. Narducci for stimulating discussions. We thank H.-J. Briegel for elucidating us the role of elastic collisions in destroying trapping states.

This research was supported by the Ministero dell' Università e della Ricerca Scientifica e Tecnologica, Italy.

REFERENCES AND NOTES

1. D. Meschede, H. Walther, and G. Müller, Phys. Rev. Lett. **54,** 551 (1985); G. Rempe, H. Walther, and N. Klein, Phys. Rev. Lett. **58,** 353 (1987); G. Rempe, F. Schmidt-Kaler, and H. Walther, Phys. Rev. Lett. **64,** 2783 (1990).
2. P. Filipowicz, J. Javanainen, and P. Meystre, Phys. Rev. A **34,** 3077 (1986).
3. E. M. Wright and P. Meystre, Opt. Lett. **14,** 177 (1989).
4. P. Meystre, G. Rempe, and H. Walther, Opt. Lett. **13,** 1078 (1988).
5. M. O. Scully, H. Walther, G. S. Agarwal, T. Quang, and W. P. Schleich, Phys. Rev. A **44,** 5992 (1991); T. Quang, G. S. Agarwal, J. Bergou, M. O. Scully, H. Walther, K. Vogel, and W. P. Schleich, Phys. Rev. A **48,** 803 (1993); K. Vogel, W. P. Schleich, M. O. Scully, and H. Walther, Phys. Rev. A **48,** 813 (1993).
6. J. Bergou, L. Davidovich, M. Orszag, C. Benkert, M. Hillery, and M. O. Scully, Phys. Rev. A **40,** 5073 (1989).
7. S.-Y. Zhu, L. Z. Wang, and H. Fearn, Phys. Rev. A **44,** 737 (1991).
8. E. S. Guerra, A. Z. Khoury, L. Davidovich, and N. Zagury, Phys. Rev. A **44,** 7785 (1991).
9. L. Davidovich, S.-Y. Zhu, A. Z. Khoury, and C. Su, Phys. Rev. A **46,** 1630 (1992).
10. J. Bergou and M. Hillery, Phys. Rev. A **49,** 1214 (1994).
11. H.-J. Briegel, B.-G. Englert, C. Ginzel, and A. Schenzle, Phys. Rev. A **49,** 5019 (1994).
12. R. Bonifacio, G. M. D'Ariano, R. Seno, and N. Sterpi, Phys. Rev. A **47,** R2464 (1993).
13. B. Daeubler, H. Risken, and L. Schoendorff, Phys. Rev. A **46,** 1654 (1992); **48,** 3955 (1993).
14. H.-J. Briegel and B.-G. Englert, Phys. Rev. A **47,** 3311 (1993).
15. R. Bellman, *Introduction to Matrix Analysis* (McGraw-Hill, New York, 1960), p. 256.
16. T. A. B. Kennedy, P. Meystre, and E. M. Wright, in *Fundamentals of Quantum Optics II,* F. Ehlotzky, ed. (Springer-Verlag, Heidelberg, 1987), p. 157.
17. P. Meystre and E. M. Wright, in *Chaos, Noise and Fractals,* R. Pike and L. A. Lugiato, eds. (Hilger, Bristol, UK, 1987), p. 102.
18. P. Filipowicz, J. Javanainen, and P. Meystre, J. Opt. Soc. Am. B **3,** 906 (1986).
19. E. T. Jaynes and F. W. Cummings, Proc. IEEE **51,** 89 (1963).
20. Note that, if damping is taken into account during atom–radiation interaction, the trapping condition (17) is slightly modified, because the Rabi frequency is changed. At zero temperature and for $2\gamma_\perp = \gamma_\parallel$, it is possible to evaluate the eigenstates of the Liouvillian operator analytically, and the modified l-photons Rabi frequency is obtained[14]: $\Omega = [g^2(l+1) - (2\gamma_c - \gamma_\parallel)^2/16]^{1/2}$.
21. Equation (18) has also been derived for low-flux one-atom masers; see, for example, Ref. 2.
22. A. M. Guzman, P. Meystre, and E. M. Wright, Phys. Rev. A **40,** 2471 (1989).